Nanoscale X-ray Tomography of Integrated Circuits using a Hybrid Electron/X-ray Microscope: Results and Prospects

Nathan Nakamura
Department of Physics
University of Colorado Boulder
Boulder, Colorado
nathan.nakamura@nist.gov
(ORCID 0000-0001-8648-0524)

Paul Szypryt
Department of Physics
University of Colorado Boulder
Boulder, Colorado
paul.szypryt@nist.gov
(ORCID 0000-0002-0184-3419)

Joseph W. Fowler
Department of Physics
University of Colorado Boulder
Boulder, Colorado
joe.fowler@nist.gov
(ORCID 0000-0002-8079-0895)

Zachary H. Levine
Quantum Optics Group
National Institute of Standards and Technology
Gaithersburg, Maryland
zlevine@nist.gov
(ORCID 0000-0002-9928-276X)

Daniel S. Swetz
Quantum Sensors Group
National Institute of Standards and Technology
Boulder, Colorado
daniel.swetz@nist.gov
(ORCID 0000-0002-8192-2175)

2023 IEEE Physical Assurance and Inspection of Electronics (PAINE) | 979-8-3503-3931-4/23/$31.00 ©2023 IEEE | DOI: 10.1109/PAINE58317.2023.10318004

***Abstract*—Accurate characterization of subsurface features in integrated circuits (ICs) is essential for defect detection, quality assurance, and supply chain security. The interiors of ICs are challenging to probe post-manufacturing due to the presence of many close-packed and nanoscale subsurface features of multiple material compositions, often spread over square millimeters of chip area. X-ray computed tomography (CT) has historically been a powerful tool for 3-dimensional imaging of buried features, but modern instruments are unable to achieve the spatial resolution, elemental sensitivity, or scan areas required to fully characterize ICs. Advanced imaging of ICs is possible at synchrotron beamlines, but such methods are not easily accessible and could not reside directly at a semiconductor foundry or security agency. A need exists for compact, laboratory-scale instrumentation that can image nanoscale features in 3-dimensions over large areas, with sensitivity to feature size, shape, and composition. We describe an approach to x-ray CT which merges a focused electron beam with high magnification system geometry and a combination of high efficiency and high resolving power x-ray detection. This achieves nanoscale, element-sensitive imaging of ICs in a compact instrument footprint. A proof-of-concept has been demonstrated and current imaging capabilities are discussed. The path forward is described, with opportunity for advances in spatial resolution, imaging speed, and spectral imaging capabilities beyond conventional laboratory CT instruments.**

***Index Terms*—Integrated circuits, x-ray computed tomography, nanoscale imaging**

I. Introduction

Modern integrated circuits (ICs) contain many close-packed, nanoscale, subsurface features of multiple material compositions spanning planar chip areas. This structural complexity has greatly improved the capabilities of ICs. However, it has also made high fidelity characterization of IC features difficult, presenting a challenge for critical IC diagnostics such as defect detection and hardware trojan identification.[1, 2] X-ray computed tomography (CT) is an ideal tool for the characterization of buried layers, providing 3-dimensional images to probe the size and shape of subsurface features.[3] However, capabilities of modern laboratory CT tools lag behind modern IC fabrication, failing to achieve the required spatial resolution and providing little to no information regarding the elemental composition. Synchrotron x-ray imaging methods have demonstrated sub-20 nm spatial resolution and represent the state-of-the-art in x-ray imaging of ICs. [4, 5] However, these methods are enabled by the high flux and coherent beam of a synchrotron x-ray source and remain significantly less accessible than their compact, laboratory-scale counterparts. A compact CT instrument holds the advantage of being able to reside directly at a semiconductor foundry or security agency, providing immediate feedback for IC analysis and troubleshooting. Thus, a need exists for a tool capable of characterizing the structural and compositional complexity of ICs in a compact, laboratory-scale footprint.

Here, we describe an approach to laboratory x-ray CT which combines the focused electron beam of a scanning electron microscope (SEM) with high magnification system geometry and both energy-resolved and high-efficiency x-ray detection (Fig. 1A). A proof-of-concept of this tool has been demonstrated and resolved 160 nm features in 6 layers of an IC while providing first steps towards elemental sensitivity in the reconstructed images.[6, 7] These capabilities are enabled in part by

The information, data, or work presented herein was funded in part by the Office of the Director of National Intelligence (ODNI), Intelligence Advanced Research Projects Activity (IARPA), via agreements D2019-1908080004, D2019-1906200003, D2021-2106170004, and FA8702-15-D-0001.

Authorized licensed use limited to: UNIVERSITY OF COLORADO. Downloaded on May 02,2024 at 18:05:43 UTC from IEEE Xplore. Restrictions apply.

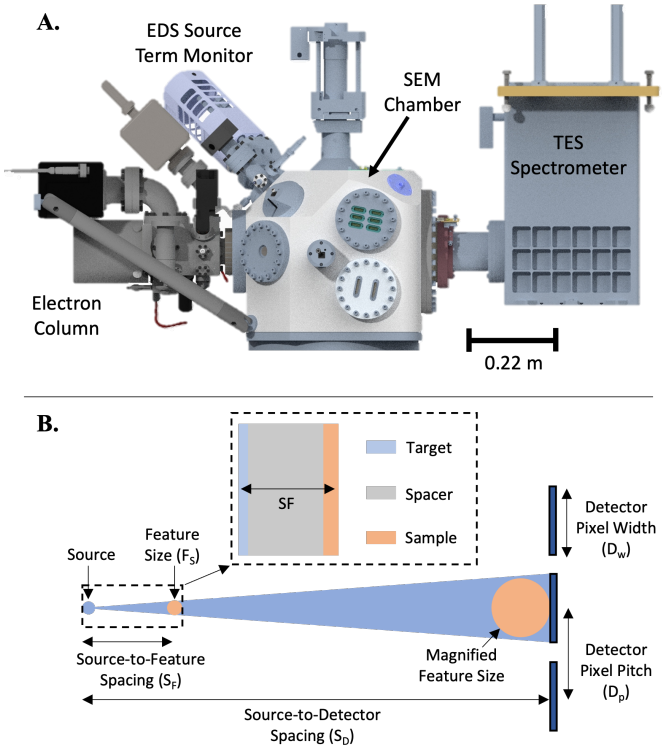

Fig. 1. A. Overview of the proof-of-concept x-ray microscope, showing the electron column, scanning electron microscope (SEM) chamber, energy dispersive x-ray spectroscopy (EDS) detector, and 240-pixel transition-edge sensor (TES) spectrometer. The TES spectrometer can be replaced with other x-ray detectors, depending on if the system is being optimized for imaging speed or spatial resolution and spectral capabilities. B. Schematic of the x-ray source, IC features, and x-ray detector, demonstrating high geometric magnification. Parts A and B have appeared in Ref. [6] and Ref. [7], respectively.

the high geometric magnification of the instrument, which is accomplished by depositing a metal target directly onto the IC sample. This provides micrometer-scale spacing between the source and sample (Fig. 1B). It allows the x-ray detector to be brought closer to the sample while maintaining high magnification, preserving a higher solid angle of collection and x-ray flux. A focused electron beam is incident on the target, generating an x-ray spot proportional to the electron beam spot size. The ability to focus electron beams to nanoscale spot sizes allows the x-ray generation volume in the target to be kept to the nanoscale, a key requirement for nanoscale x-ray CT. A transition-edge sensor (TES) spectrometer is used for x-ray detection, due to their combination of high resolving power and good collection efficiency.[8] An energy resolving detector allows energy bands to be selected which contain characteristic photons that are generated predominantly in the nanoscale spot size in the target, rather than including background x-rays not generated in the target which have spread to a larger spot size. Additionally, energy bands can be selected to promote high contrast for specific materials in the IC, allowing for increased elemental sensitivity.[9, 10] Additional details on system design can be found in [6].

This approach to x-ray CT fundamentally changes existing limitations, offering an alternative path to higher spatial resolutions, IC chip-relevant scan areas, and spectral imaging capabilities. To achieve nanoscale spatial resolution, the x-ray focal spot size must be kept comparable to the desired spatial resolution while maintaining enough flux for suitable signal-to-noise. The spot size and generated flux in a conventional CT experiment is limited by the x-ray tube source and x-ray focusing optics, while here the spot size is limited by electron beam focusing and target deposition. Electron beams can routinely be focused to nanoscale spot sizes and thin film fabrication techniques can deposit target layers with nanometer-scale control, providing tunable, nanoscale x-ray spot sizes based on electron beam and target parameters. Additionally, imaging large planar areas is not possible in conventional laboratory nanoscale CT, as a reliance on destructive sample preparation techniques eliminates all but a micrometer-scale area of the IC.[11] Here, the planar thin film target held micrometers from the sample allows the planar IC geometry to be kept intact, enabling full-chip or large area scanning. Lastly, spectral tomography methods which yield information on the elemental or chemical composition of the sample rely on the ability to resolve multiple energy bands or specific fluorescence lines.[9, 10, 12] Generally, x-ray CT instruments use high efficiency x-ray detection with poor or no energy resolution, severely limiting any path forward for spectral imaging. The x-ray microscope described here is compatible with both high efficiency and high resolving power detection, and modes focusing on spectral capabilities will be possible.

In this report, results from a recent proof-of-concept measurement and the current capabilities of the x-ray microscope will be briefly discussed. Then, paths towards higher spatial resolution, faster imaging speed, and enhanced spectral imaging capabilities will be shown. We anticipate that the fully realized instrument will achieve large area scans of planar ICs with on order 100 nm spatial resolution using highly efficient, but poorly energy resolved x-ray detection. This scan will be used to identify additional regions-of-interest, which will be scanned at 10s of nanometer spatial resolution with elemental sensitivity using energy-resolving x-ray detectors. The current instrument is already a powerful tool for nanoscale IC imaging, and we anticipate future iterations will provide new imaging capabilities for modern IC characterization.

II. Current Performance

A proof-of-concept was demonstrated on an IC sample with predominantly Cu features and a 160 nm minimum feature size. The IC design file was used for comparison with the resulting reconstructions to verify instrument performance, but was not used as an input to guide image generation (Fig. 2A). The advantages of energy-resolving x-ray detection in tomography were shown using a 240-pixel TES spectrometer, which enabled high spatial resolution and demonstrated the first steps towards element-specific reconstructions. In Figure 2B, a reconstruction of multiple IC wiring and via layers is shown using the 9.1-10.1 keV energy band. This band

Authorized licensed use limited to: UNIVERSITY OF COLORADO. Downloaded on May 02,2024 at 18:05:43 UTC from IEEE Xplore. Restrictions apply.

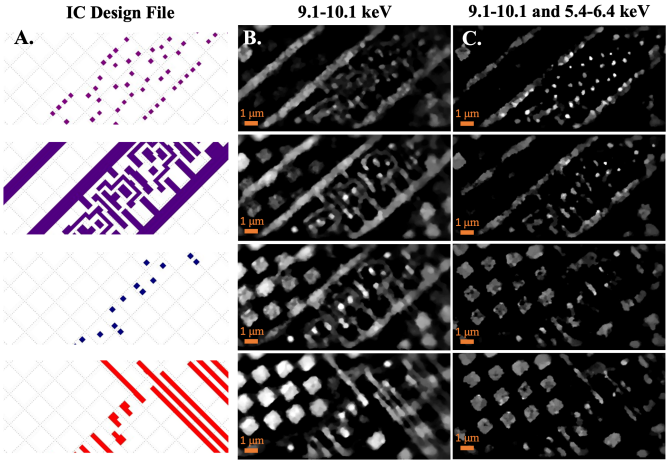

Fig. 2. A. The design file for the demonstration IC, showing 4 of the wiring and via layers imaged. B. Reconstruction using only the 9.1-10.1 keV energy band, which contains the Pt Lα fluorescence line originating in the target material. C. Reconstruction using the 9.1-10.1 keV and 5.4-6.4 keV energy bands. Inclusion of the lower energy band enhances contrast for non-Cu IC features. The large diamond-shaped features in the reconstruction are chemical-mechanical polishing (CMP) filling, which is an IC feature added for thermal and mechanical stability but is not included in the design file here.[13] Portions of this figure have appeared in Refs. [6] and [7]

is dominated by the Pt Lα line, and thus originates mostly in the Pt target used for this data collection. All expected features are clearly resolved, demonstrating that the spatial resolution is at least 160 nm. In Figure 2C, a reconstruction including both the 9.1-10.1 keV and 5.4-6.4 keV energy bands is shown. The lower energy band enhances contrast for non-Cu features and the resulting reconstruction shows higher contrast for the first via layer relative to other wiring and via layers, indicating the presence of non-Cu vias in the IC. These results demonstrated the promise of combining a focused electron beam, high system magnification, and energy-resolved x-ray detection for nanoscale x-ray tomography. Additional explanation and results can be found in Ref. [6] and Ref. [7].

III. Methods

Methods for data collection and tomographic reconstruction have been published previously.[6, 7] Monte Carlo electron-photon transport modeling is presented here to describe future design and system performance considerations. Modeling was done using the PENELOPE (Penetration and ENErgy LOss of Positrons and Electrons) code package, version 2018, driven via the main program PENEPMA.[14, 15] Pt and Ti targets were simulated. Pt was found to maximize imaging speed in the prior data collection, and Ti is included here to provide a comparison to lower atomic number target materials. A 25 keV electron pencil beam was used to generate x-rays in the target layers. While other accelerating voltages can be chosen experimentally, 25 keV was found to be a suitable choice to maximize imaging speed while maintaining small spot sizes. When predicting the x-ray spot size, the electron beam is convolved with a gaussian beam shape to obtain estimates of the x-ray spot full-width half-maximum (FWHM). When predicting imaging speed, the electron beam current, detector collection efficiency, detector solid angle of collection, and detector dynamic range are taken into account.

IV. Future Outlook

The approach to x-ray nanotomography presented here has a promising future, with a path towards improved imaging speed, spatial resolution, and spectral imaging capabilities. As instrument performance is pushed forward, compromises with respect to the imaging speed and spatial resolution will guide decisions regarding the electron beam, target design, and x-ray detector. When selecting electron beam parameters, a larger beam current will produce more x-ray flux, but also result in a larger electron beam spot. Thus, imaging speed would be improved at the cost of spatial resolution. A similar constraint exists for target design. Thicker targets will improve x-ray flux from the target layer, but produce a larger x-ray generation volume and thus a larger focal spot size. In general, source design decisions that enhance the imaging speed will degrade the spatial resolution, and improving spatial resolution will result in slower imaging speeds. Given these competing requirements, a system with the flexibility to be optimized for imaging speed or spatial resolution is desirable. In this instrument, opportunities exist to improve the imaging speed by orders of magnitude and push the spatial resolution to the order of 10s of nanometers.

To achieve this goal, upgrades to existing system components are necessary. The electron column used in the previous demonstration was designed for SEM imaging, while the goal of an x-ray microscope electron column should be to produce as many electrons in as small a spot as possible. Electron columns can reach microamperes of beam current,[16] orders of magnitude above the previously used beam current. Electron beam parameters can be adjusted during microscope operation, allowing for tunable spot size and beam current based on the imaging goals of a specific IC sample. Target fabrication can also be adjusted to optimize for a given spatial resolution goal and sample composition. Source upgrades and optimization will be critical for future experiments, as it will set the x-ray spot size and flux. However, electron beams can routinely reach nanometer-scale spot sizes and target fabrication is controllable at the nanometer-scale, providing ample room for optimization. The final capabilities of a fully realized instrument may ultimately be set by the capabilities of the x-ray detector. As with other system parameters, the choice of detector will impact both the achievable imaging speed and spatial resolution. When optimizing for imaging speed, it is advantageous to utilize a highly efficient x-ray detector to maximize the detected count rate. When optimizing for spatial resolution, the requirement that the majority of photons be generated in the target layer may necessitate energy-resolved x-ray detection. If spectral capabilities are desired, energy-resolved x-ray detection will be essential. These considerations will be discussed in more detail in subsequent sections.

We compare the performance of 3 detectors, all of which have been or are currently being integrated into the instrument:

Authorized licensed use limited to: UNIVERSITY OF COLORADO. Downloaded on May 02,2024 at 18:05:43 UTC from IEEE Xplore. Restrictions apply.

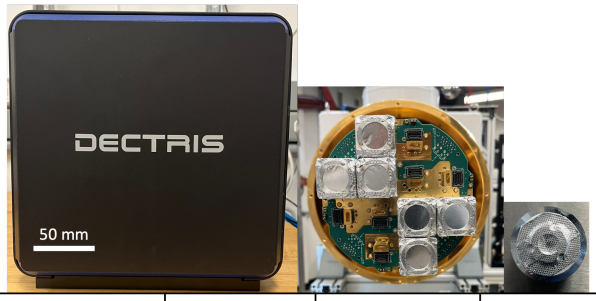

	Dectris Eiger2	3,000-pixel TES	240-pixel TES
Active Area (mm²)	25,157	499	23
Efficiency at 9.4 keV	0.98	0.84	0.44
Energy Resolution at 9.4 keV (eV)	N/A, 2 energy thresholds	10	25
Imaging Speed Improvement Factor	1,000	50	N/A

Fig. 3. The Dectris Eiger2, 3,000-pixel TES, and 240-pixel TES, shown to scale from left to right. The Eiger2 is shown with a protective cover, while the TES pixels are covered by aluminum filters. 1,500 pixels of the final 3,000-pixel TES system are shown (middle), as the spectrometer is still under development. The Eiger2 provides significantly more active collection area and a higher collection efficiency in the x-ray energy range of interest, but can only distinguish photon energy based on 2 energy thresholds. The 3,000-pixel TES will provide an upgrade over the 240-pixel system with regards to active area, collection efficiency, and energy resolution.

a Dectris Eiger2, a 3,000-pixel TES spectrometer, and a 240-pixel TES spectrometer. The Eiger2 is a commercial hybrid photon-counting detector.[17] It utilizes 450 μm thick Si pixels with high detection efficiency, but has energy resolving capabilities limited to the use of 2 energy thresholds. The 240-pixel TES spectrometer was used for the previous imaging demonstration.[18, 19] While it demonstrated the power of energy-resolved detection and provided enough collection efficiency for imaging, it has relatively low collection efficiency compared to other detectors used for x-ray CT. To enable energy-resolved detection and spectral imaging in future measurements, a 3,000-pixel TES spectrometer is under development which will improve both the collection efficiency and energy resolution compared to the 240-pixel system.[20, 21] A comparison of all 3 detectors is shown in Figure 3. During data collection, we anticipate that these detectors could be easily exchanged for one another based on a given IC sample or imaging goal. Which detector is chosen will depend on whether the application calls for optimal imaging speed, spatial resolution, or spectral capabilities.

A. Imaging Speed

Imaging speed is an important consideration for any x-ray CT instrument, as it sets the data collection time for a given scan area. An estimate of how each x-ray detector would affect the imaging speed was made, using the 240-pixel TES data collection as the reference point. PENELOPE was used to obtain the predicted count rate for each detector. Compared to the 240-pixel TES, the Eiger2 and 3,000-pixel TES are estimated to be about 1,000 and 50 times faster, respectively (Fig. 3). It is also expected that an upgraded electron column could significantly increase the achievable beam current and thus significantly increase the imaging speed. Additionally, methods are under development which would reduce the number of photons required for high signal-to-noise reconstructions.[22–24] These photon-starved reconstructions could result in much faster data collection times in the future.

The Eiger2 is the ideal choice when optimizing the instrument for imaging speed and will be the detector of choice for larger area scans. However, its lack of energy resolution could limit the achievable spatial resolution. The inability to select for photons generated in the target with high precision necessitates that the majority of photons be generated in the target layer for the Eiger2 to be successful. If a large portion of the detected photons are generated in a larger spot outside of the target layer, the spatial resolution will be degraded. This puts tight constraints on the electron beam and target parameters when pushing the spatial resolution to the 10s of nanometers level. The next section will discuss these constraints and how energy resolved detection may be necessary for data collection at the highest spatial resolutions.

B. Spatial Resolution

The spatial resolution sets the smallest IC feature size that can be observed. Multiple instrument factors influence this, including the system magnification, x-ray detector geometry, and the focal spot size.[25, 26] In general, it is desirable to have a focal spot size comparable to the smallest feature size in the sample. As the focal spot size gets larger, additional image blurring will occur.[27] For high magnification systems, the source focal spot size is the dominant factor determining the achievable spatial resolution.[28, 29] In our approach to x-ray CT, the focal spot size is set by the electron beam size and the target thickness. Ideally, all detected photons would originate in the nanoscale volume generated in the target layer, allowing for every photon to contribute to the reconstruction without degrading image quality. In reality, many detected photons originate outside the target layer. Electrons from the

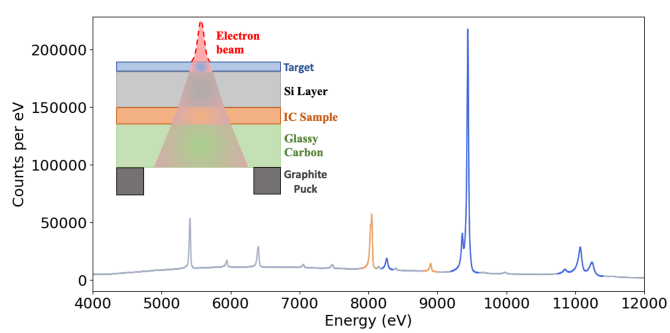

Fig. 4. A TES spectrum demonstrating the broadband collection and energy resolution of the 240-pixel TES spectrometer. The inset shows a schematic of x-ray generation in the target and other layers of the sample. A nanofocused spot is generated in the target layer, while photons generated in other layers originate in a larger, more disperse spot size. Pt and Cu fluorescence lines in the spectrum are shown in blue and orange, respectively. Background from other sample layers and materials in the SEM chamber are shown in grey. A modified version of the inset was shown in Ref. [6].

Authorized licensed use limited to: UNIVERSITY OF COLORADO. Downloaded on May 02,2024 at 18:05:43 UTC from IEEE Xplore. Restrictions apply.

TABLE I

THE PERCENT BEAM SPREAD, X-RAY SPOT SIZE, AND PERCENT OF PHOTONS GENERATED IN THE TARGET LAYER FOR 3 DIFFERENT TARGETS OF VARYING THICKNESS AND MATERIAL. THE INCIDENT ELECTRON BEAM IS ASSUMED TO BE A 50 NM FWHM GAUSSIAN BEAM.

	50 nm Pt Target	**100 nm Pt Target**	**100 nm Ti Target**
Percent Beam Spread	10.8	30.0	5.6
X-ray Spot Size (nm)	55	65	53
Percent from Target	42	65	11

incident beam will spread to a more disperse spot size after the target layer, generating additional photons from a larger spot in other layers of the sample (Fig. 4, inset). When the target is thick, most photons will be generated in the target, with the caveat that the generation volume inside the target will be larger. As the target gets thinner, the x-ray generation volume in the target will decrease, improving the achievable spatial resolution. However, more photons will also be generated in non-target layers from a larger spot size. These non-target photons will degrade the spatial resolution if included in the reconstruction. As target materials are pushed thinner to accommodate lower spatial resolution goals, a point may be reached where energy-resolved detection becomes necessary due to a large proportion of detected x-rays being generated outside of the target layer.

The electron beam conditions, target thickness, and target material should be selected based on the expected spot size and what proportion of x-rays are expected to originate in the target layer. An example TES spectrum from the 240-pixel spectrometer is shown in Figure 4 to demonstrate how energy-resolving x-ray detection can select for spectral regions which originate in specific layers of the sample. If the spot size is comparable to the smallest IC feature sizes and the majority of photons still originate in the target layer, it is acceptable to use a detector like the Eiger2 which does not provide precise energy resolution. If, however, the IC feature sizes necessitate a smaller spot size and thinner target such that the majority of detected x-rays are generated outside of the target layer, it will become necessary to use energy-resolving detectors like TES spectrometers to select energy bins predominantly composed of target photons. TES spectrometers could thus be used for the highest possible spatial resolution scans, under the constraint that scan areas will be limited due to the decrease in collection efficiency relative to a detector like the Eiger2. It has not been determined exactly where the transition point between detectors will occur when optimizing for spatial resolution; that will be the topic of future studies.

To explore this concept, PENELOPE simulations were performed for Pt and Ti targets ranging in thickness from 50 nm to 100 nm to determine the x-ray spot size and the percent of photons generated in the target layer. As an example, we explore the use-case of a 50 nm FWHM electron beam incident

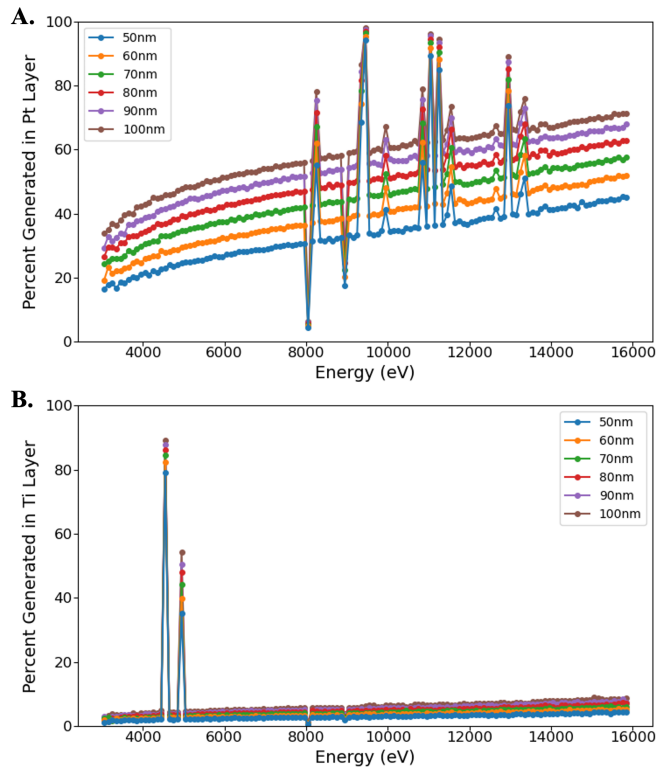

Fig. 5. The percent of photons generated in a Pt (A) and Ti (B) target versus energy bin for various target thicknesses. Energy bins are 100 eV wide, but could be much smaller when using a TES spectrometer. In both plots, the bins that contain the fluorescence lines from the target material have a higher proportion of generated photons originating in the target material. Thicker and higher atomic number targets lead to more photons generated in the target.

on a 100 nm Pt target, a 50 nm Pt target, and a 100 nm Ti target (Table I). In the 100 nm Pt target, the x-ray spot size is estimated to be approximately 65 nm. With a 50 nm Pt target the x-ray spot size is only 55 nm, allowing smaller IC features to be resolved. However, 65% of all photons are generated in the target for the 100 nm thick Pt, while only 42% originate in the target for the 50 nm thick Pt. Thus, if all photons are used for the 50 nm target rather than using an energy resolving detector to select for the Pt fluorescence lines, many photons outside of the 55 nm x-ray spot will be included in the reconstruction and introduce additional feature blurring. In a lower atomic number material like Ti, the target stops fewer electrons and thus the x-ray spot size remains smaller. For the 100 nm Ti target, the estimated x-ray spot size is 53 nm. However, the lower stopping power also reduces the amount of photons generated in the target, as only 11% of photons were generated in the target layer.

Energy-resolved detection can select for the characteristic lines of the target material, ensuring that the spot size used is limited to the generation volume in the target. However, selecting for only fluorescence lines will reduce the total counts used in the reconstruction, negatively impacting the signal-to-noise. It can be advantageous to include non-fluorescence photons to increase the total photon count, provided that the

Authorized licensed use limited to: UNIVERSITY OF COLORADO. Downloaded on May 02,2024 at 18:05:43 UTC from IEEE Xplore. Restrictions apply.

majority of the photons were generated in the target layer. In this case, it is desirable to know which energy bins have the highest proportion of x-rays generated in the target and how wide those bins can be before non-target photons dominate the reconstruction. Figure 5A-B shows the percent of x-rays generated in Pt and Ti targets for 100 eV wide energy bins ranging from 3 to 16 keV. As expected, the bins containing the fluorescence lines have the highest percentage of target x-rays. In the Pt target, it is also apparent that higher energy bins are more advantageous to include than lower energy bins in the absence of a fluorescence line, as the higher energy bins have more photons from the target layer. This is not the case for Ti, where very few photons originate in the target outside of the characteristic line. With a Ti or other lower atomic number target, it would be more detrimental to the spatial resolution to include non-fluorescence photons in the reconstruction, as the majority of non-fluorescence photons originate outside of the target regardless of which energy bins are used. Therefore, lower resolving power may be acceptable when using higher atomic number targets like Pt, since many photons will originate in the target layer even outside of the fluorescence line. In lower atomic number targets, it will be necessary to select for fluorescence lines. When selecting for the characteristic lines, detectors with higher resolving power will discriminate between the fluorescence line and background with higher signal-to-noise, thus including less non-target photons and improving the spatial resolution. In general, energy-resolving detectors like TES spectrometers can be used to select for energy bins which are predominantly composed of photons generated in the nanoscale volume in the target, helping to maximize the total usable count rate while maintaining the desired spatial resolution.

C. Spectral Imaging

Spectral x-ray CT adds elements of x-ray spectroscopy to x-ray CT, using energy and material-dependent information to determine elemental composition or chemical speciation in each voxel. In simpler cases, such as enhancing the contrast between materials of different composition, this requires the ability to collect data with multiple distinct energy bins.[9, 10] In more advanced spectral imaging cases which utilize the absorption edges or fluorescence emission of a sample, a detector with higher resolving power is required.[12] In our instrument, the TES spectrometer would be required for any spectral imaging applications. A TES spectrometer is an ideal tool for such a task, as it can efficiently collect a broadband spectrum with high energy resolution. This allows for observation of many spectral features simultaneously and enables many distinct energy bins to be input to the reconstruction. A larger number of energy bins can enhance contrast between different elements and identify more distinct materials composing the IC sample.[30] The use of spectral features such as absorption edges or emission lines for spectral tomography has largely been limited to synchrotron facilities, and is not readily available in any laboratory CT instrument.[31, 32] However, TES spectrometers have long been utilized for x-ray spectroscopy,[8, 33, 34] and have a history of successfully bringing synchrotron spectroscopic techniques to the laboratory scale.[35, 36] Additionally, the TES spectrometer could be utilized with novel, multi-material target designs to select for fluorescence lines only from specific target materials during reconstruction, selectively enhancing the contrast of certain IC components based on their energy-dependent x-ray attenuation. Our proof-of-concept showed first steps toward elemental selectivity with the 240-pixel TES spectrometer and a single-material Pt target, and we expect these capabilities to become more advanced with the 3,000-pixel spectrometer integration and advances in reconstruction codes.

V. Conclusion

An approach to x-ray CT of ICs is introduced using a focused electron beam and thin film metal target source, high geometric magnification, and multiple types of x-ray detectors. A prior proof-of-concept measurement resolved 160 nm features in an IC and presented first steps towards elemental sensitivity. In future iterations, optimization of the electron column, target design, and x-ray detection method will enable vastly improved imaging speed, spatial resolution, and spectral imaging capabilities. We envision an x-ray tomography instrument able to scan large IC areas with approximately 100s of nanometer spatial resolution using an x-ray detector with high collection efficiency, but poor energy resolving capabilities. This large area scan can be used to identify specific regions-of-interest, which would be investigated at 10s of nanometer spatial resolution with spectral imaging capabilities using energy-resolved x-ray detectors. The end goal is an x-ray nanotomography instrument capable of advanced IC characterization, providing information on nanoscale feature size, shape, and composition across planar chip areas.

Acknowledgment

The authors thank all team members who contributed to the development of and data collection using the proof-of-concept instrument, from both NIST and Sandia National Laboratories. Mention of commercial products does not imply endorsement by the authors or their institutions. The views and opinions of authors expressed herein do not necessarily state or reflect those of the United States Government or any agency thereof.

References

[1] P. Aryan, S. Sampath, and H. Sohn, "An overview of non-destructive testing methods for integrated circuit packaging inspection", Sensors **18**, 10.3390/s18071981 (2018).

[2] A. Jain, Z. Zhou, and U. Guin, "Survey of recent developments for hardware trojan detection", in 2021 ieee international symposium on circuits and systems (iscas) (2021), pp. 1–5.

[3] P. J. Withers et al., "X-ray computed tomography", Nature Reviews Methods Primers **1**, 18 (2021).

[4] M. Holler, M. Guizar-Sicairos, E. H. R. Tsai, R. Dinapoli, E. Muller, O. Bunk, J. Raabe, and G. Aeppli, "High-resolution non-destructive three-dimensional imaging of integrated circuits", Nature **543** (2017).

Authorized licensed use limited to: UNIVERSITY OF COLORADO. Downloaded on May 02,2024 at 18:05:43 UTC from IEEE Xplore. Restrictions apply.

[5]M. Holler et al., "Three-dimensional imaging of integrated circuits with macro- to nanoscale zoom", Nature Electronics **2**, 464–470 (2019).

[6]N. Nakamura et al., "A tabletop x-ray tomography instrument for nanometer-scale imaging: integration of a scanning electron microscope with a transition-edge sensor spectrometer", arXiv, https://arxiv.org/abs/2212.10591 (2023).

[7]Z. H. Levine et al., "A tabletop x-ray tomography instrument for nanometer-scale imaging: reconstructions", Microsystems & Nanoengineering **9** (2023).

[8]J. N. Ullom and D. A. Bennett, "Review of superconducting transition-edge sensors for x-ray and gamma-ray spectroscopy", Superconductor Science and Technology **28**, 084003 (2015).

[9]C. H. McCollough, S. Leng, L. Yu, and J. G. Fletcher, "Dual- and multi-energy CT: principles, technical approaches, and clinical applications", Radiology **276**, 637–653 (2015).

[10]P. M. Shikhaliev, "Computed tomography with energy-resolved detection: a feasibility study", Physics in Medicine and Biology **53**, 1475–1495 (2008).

[11]C. Tan et al., "Rapid preparation of geometrically optimal battery electrode samples for nano scale x-ray characterisation", Journal of The Electrochemical Society **167**, 060512 (2020).

[12]S. Feng, E. Liotti, M. D. Wilson, L. Jowitt, and P. S. Grant, "In situ mapping of chemical segregation using synchrotron x-ray imaging", MRS Bulletin **45**, 934–942 (2020).

[13]D. Zhao and X. Lu, "Chemical mechanical polishing: theory and experiment", Friction **1**, 306–326 (2013).

[14]NEA, *PENELOPE 2018: a code system for Monte Carlo simulation of electron and photon transport* (2019).

[15]X. Llovet and F. Salvat, "PENEPMA: a Monte Carlo program for the simulation of x-ray emission in electron probe microanalysis", Microscopy and Microanalysis **23**, 634–646 (2017).

[16]T. Kusunoki, T. Hashizume, K. Kasuya, and N. Arai, "Stabilization of cold-field-emission current from a CeB6 single-crystal emitter by using a faceted (100) plane", Journal of Vacuum Science & Technology B **39** (2020).

[17]A. Förster, S. Brandstetter, and C. Schulze-Briese, "Transforming x-ray detection with hybrid photon counting detectors", Philosophical Transactions of the Royal Society A **377**, 20180241 (2019).

[18]W. B. Doriese et al., "A practical superconducting-microcalorimeter x-ray spectrometer for beamline and laboratory science", Review of Scientific Instruments **88**, 053108 (2017).

[19]C. G. Pappas et al., *A TES x-ray spectrometer for NSENSE*, tech. rep. (National Institute of Standards and Technology Boulder United States, 2019).

[20]P. Szypryt et al., "A tabletop x-ray tomography instrument for nanometer-scale imaging: demonstration of the 1,000-element transition-edge sensor subarray", IEEE Transactions on Applied Superconductivity **33**, 1–5 (2023).

[21]P. Szypryt et al., "Design of a 3000-pixel transition-edge sensor x-ray spectrometer for microcircuit tomography", IEEE Transactions on Applied Superconductivity **31**, 1–5 (2021).

[22]Z. Guo, Z. Liu, G. Barbastathis, Q. Zhang, M. E. Glinsky, B. K. Alpert, and Z. H. Levine, "Noise-resilient deep learning for integrated circuit tomography", Opt. Express **31**, 15355–15371 (2023).

[23]Z. Guo, J. K. Song, G. Barbastathis, M. E. Glinsky, C. T. Vaughan, K. W. Larson, B. K. Alpert, and Z. H. Levine, "Physics-assisted generative adversarial network for x-ray tomography", Opt. Express **30**, 23238–23259 (2022).

[24]J. Song, Z. H. Levine, B. K. Alpert, M. E. Glinsky, J. W. Fowler, and G. Barbastathis, "Information theoretic study on x-ray imaging of integrated circuits in a low photon budget", in Osa imaging and applied optics congress 2021 (3d, cosi, dh, isa, pcaop) (2021), CTu2F.7.

[25]K. A. Mohan, R. M. Panas, and J. A. Cuadra, "Saber: a systems approach to blur estimation and reduction in x-ray imaging", IEEE Transactions on Image Processing **29**, 7751–7764 (2020).

[26]J. Wang and D. Fleischmann, "Improving spatial resolution at ct: development, benefits, and pitfalls", Radiology **289**, PMID: 29944083, 261–262 (2018).

[27]B. Nielsen, *Resolution, unsharpness and mtf*, 1980.

[28]J. Rueckel, M. Stockmar, F. Pfeiffer, and J. Herzen, "Spatial resolution characterization of a x-ray microct system", Applied Radiation and Isotopes **94**, 230–234 (2014).

[29]J. Coenen, E. Tchouparova, X. Jing, et al., "Measurement parameters and resolution aspects of micro x-ray tomography for advanced core analysis", in Proceedings of international symposium of the society of core analysts (2004).

[30]J. Fornaro et al., "Dual-and multi-energy ct: approach to functional imaging", Insights into Imaging **2**, 149–159 (2011).

[31]D. L. Howard et al., "The XFM beamline at the Australian Synchrotron", Journal of Synchrotron Radiation **27**, 1447–1458 (2020).

[32]A. Somogyi, R. Tucoulou, G. Martinez-Criado, A. Homs, J. Cauzid, P. Bleuet, S. Bohic, and A. Simionovici, "ID22: a multitechnique hard X-ray microprobe beamline at the European Synchrotron Radiation Facility", Journal of Synchrotron Radiation **12**, 208–215 (2005).

[33]J. Ullom et al., "Transition-edge sensor microcalorimeters for x-ray beamline science", Synchrotron Radiation News **27**, 24–27 (2014).

[34]L. Miaja-Avila et al., "Valence-to-core x-ray emission spectroscopy of titanium compounds using energy dispersive detectors", X-Ray Spectrometry **50**, 9–20 (2021).

[35]Y. I. Joe, G. C. O'Neil, L. Miaja-Avila, J. W. Fowler, R. Jimenez, K. L. Silverman, D. S. Swetz, and J. N. Ullom, "Observation of iron spin-states using tabletop x-ray emission spectroscopy and microcalorimeter sensors", Journal of Physics B: Atomic, Molecular and Optical Physics **49**, 024003 (2015).

[36]L. Miaja-Avila et al., "Ultrafast time-resolved hard x-ray emission spectroscopy on a tabletop", Phys. Rev. X **6**, 031047 (2016).

Authorized licensed use limited to: UNIVERSITY OF COLORADO. Downloaded on May 02,2024 at 18:05:43 UTC from IEEE Xplore. Restrictions apply.